NANO LETTERS
Cite This: Nano Lett. 2017, 17, 7638−7646
Letter
pubs.acs.org/NanoLett

Deterministic Line-Shape Programming of Silicon Nanowires for Extremely Stretchable Springs and Electronics

Zhaoguo Xue,[†] Mei Sun,[‡] Taige Dong,[†] Zhiqiang Tang,[‡] Yaolong Zhao,[†] Junzhuan Wang,[†] Xianlong Wei,*[,‡] Linwei Yu,*[,†,§] Qing Chen,[‡] Jun Xu,[†] Yi Shi,[†] Kunji Chen,[†] and Pere Roca i Cabarrocas[§]

[†]National Laboratory of Solid State Microstructures/School of Electronic Science and Engineering/Collaborative Innovation Center of Advanced Microstructures, Nanjing University, 210093 Nanjing, People's Republic of China

[‡]Key Laboratory for the Physics and Chemistry of Nanodevices/Department of Electronics, Peking University, 100871 Beijing, People's Republic of China

[§]LPICM, CNRS, Ecole Polytechnique, Université Paris-Saclay, 91128 Palaiseau, France

Supporting Information

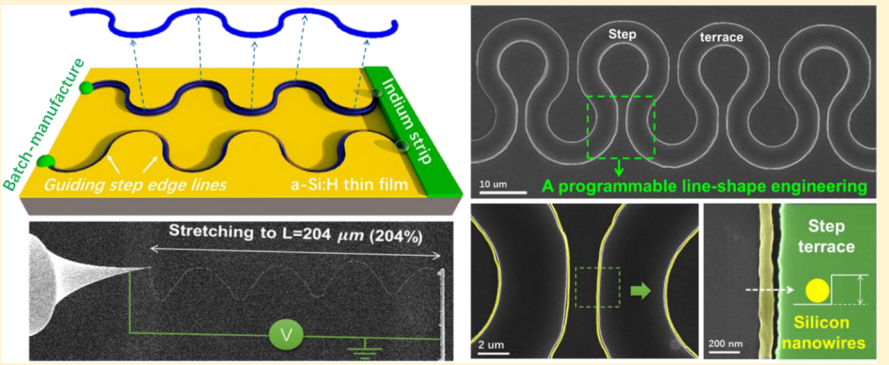

ABSTRACT: Line-shape engineering is a key strategy to endow extra stretchability to 1D silicon nanowires (SiNWs) grown with self-assembly processes. We here demonstrate a deterministic line-shape programming of in-plane SiNWs into extremely stretchable springs or arbitrary 2D patterns with the aid of indium droplets that absorb amorphous Si precursor thin film to produce ultralong c-Si NWs along programmed step edges. A reliable and faithful single run growth of c-SiNWs over turning tracks with different local curvatures has been established, while high resolution transmission electron microscopy analysis reveals a high quality monolike crystallinity in the line-shaped engineered SiNW springs. Excitingly, in situ scanning electron microscopy stretching and current−voltage characterizations also demonstrate a superelastic and robust electric transport carried by the SiNW springs even under large stretching of more than 200%. We suggest that this highly reliable line-shape programming approach holds a strong promise to extend the mature c-Si technology into the development of a new generation of high performance biofriendly and stretchable electronics.

KEYWORDS: *In-plane silicon nanowires, line-shape engineering, stretchable electronics*

Crystalline silicon (c-Si) is the dominant semiconducting material that underpins the development of modern microelectronics but falls short of sustaining large bending and stretching that are encountered in deploying biocomfortable sensors and electronics upon soft or curvilinear skins or tissue surfaces.[1−6] So far, most of the stretchable electronics have been prototyped and fabricated with polymer and organic semiconductors,[7−12] which usually offers poorer electronic characteristics compared to those of c-Si based devices, particularly in terms of carrier mobility, passivation and stability in air/humidity exposure.[8,12] Recently, there have been many pioneering efforts devoted to forging stretchable c-Si channels, by elaborated electron beam lithography (EBL), etching and patterning of monocrystalline Si layers based on silicon-on-insulator (SOI) structures, into elastic 2D ribbons, serpentine, and fractal layouts.[13−15] Moreover, with the aid of the contractive strain of attached elastomer, buckled 3D out-of-plane c-Si wrinkles[16−18] or sinusoidal Si nanowires (SiNWs), grown via vapor−liquid−solid (VLS) mode,[19,20] can be prepared to better accommodate large stretching strain.[21−23] In addition, VLS growth of Si or Ge NWs with ab initio controlled shapes can be accomplished by confining the one-dimensional (1D) growth within EBL-defined nanochannels, where the guiding channels by themselves have to be as thin as

Received: August 25, 2017
Revised: October 30, 2017
Published: November 30, 2017

DOI: 10.1021/acs.nanolett.7b03658
Nano Lett. 2017, 17, 7638−7646

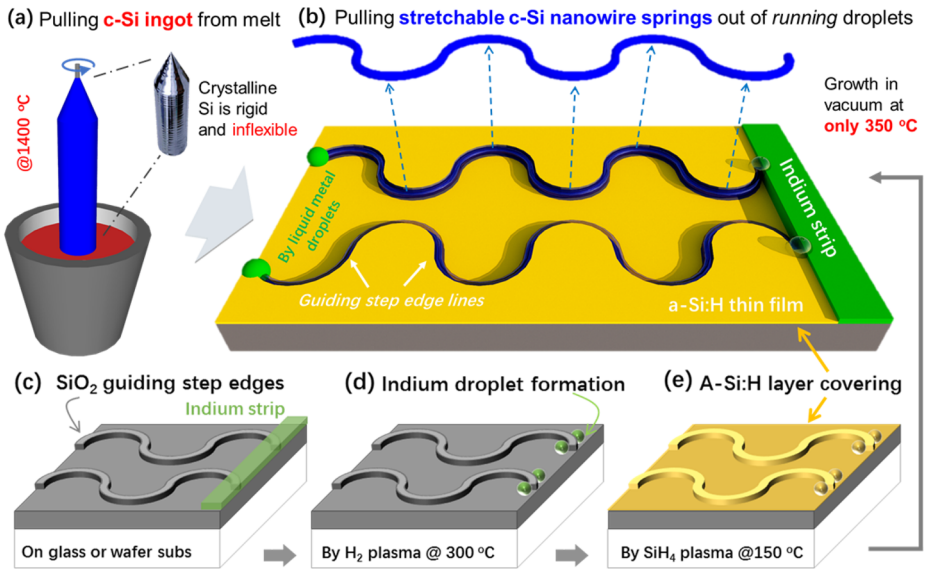

Figure 1. Illustrations for the in-plane growth of SiNWs along step edges. (a,b) Comparing the crystalline Si pulling from Si liquid at 1400 °C to a programmable pulling growth of c-Si NWs from surface-running catalyst liquid droplets at only 350 °C, absorbing amorphous Si thin film as precursor; panels c–e and b depict schematically the fabrication procedure of the in-plane SiNWs.

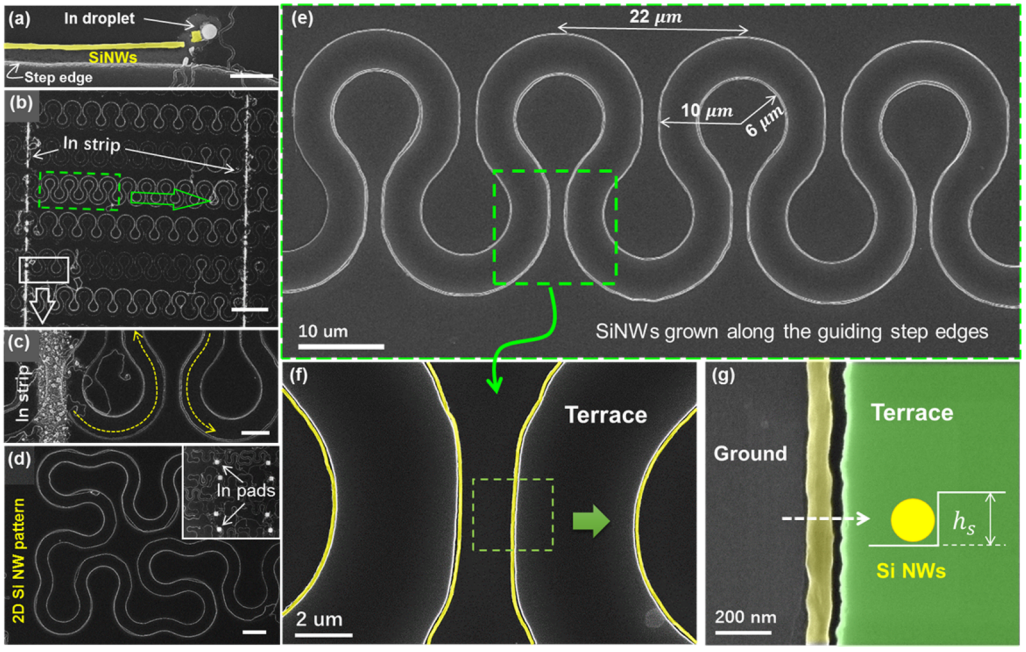

Figure 2. Line-shape engineering of in-plane Si nanowires (SiNW) where panel a shows a scanning electron microscopy (SEM) image of an in-plane SiNW led by an In droplet along the guiding step edge line; panel b presents an SEM overview of an array of SiNWs grown into programmable horseshoe patterns, starting from the vertical In strips. A close scrutiny of the initial kicking off growth from the In strip is provided in (c). The scale bars in (a–c) are 1, 40, and 5 μm, respectively. A series of enlarged views of the SiNWs grown in a region marked by the green dashed rectangles are provided in (e–g), where the SiNWs along the step edges are highlighted by pseudocolor of yellow for clarity. Finally, a 2D Peano SiNW pattern can be grown by a single ultralong SiNW as witnessed in (d). The scale bars in (d–g) are 10 μm, 10 μm, 2 μm, and 200 nm, respectively.

the SiNWs with diameters of 80–120 nm.[24] However, the use of EBL is expensive and unaffordable for large area electronics, while the postgrowth transferring and buckling are intrinsically challenging and risky. Ideally, a natural self-assembly growth of c-Si NWs out of the leading catalyst liquid droplets, in a way similar to the crystal pulling of ingot from molten Si as depicted in Figure 1a, can help to guarantee a continuous and coherent lattice ordering in the c-Si channels. While this is almost impossible in large scale crystal pulling control, the line-shape engineering of SiNWs can be readily predefined thanks to a reliable manipulation or steering control over the leading liquid metal droplet, as illustrated schematically in Figure 1b.

Though self-assembly growth has been known to produce crystalline Si NWs with a rich set of geometries, such as springs and coils,[25−31] most of them are obtained as randomly distributed arrays or bundles, which are hard to position and integrate. In this work, we propose and demonstrate a deterministic line-shape programming of ultralong in-plane SiNWs into extremely stretchable c-Si springs or arbitrary singly connected 2D fractal patterns without the need of high

DOI: 10.1021/acs.nanolett.7b03658
Nano Lett. 2017, 17, 7638–7646

resolution EBL patterning. This has been accomplished by directing the in-plane movement of In catalyst droplets along the predesigned step edge lines, via a low temperature in-plane solid−liquid−solid (IPSLS) growth mechanism,[32,33] where a coherent crystalline lattice is guaranteed in the ultralong SiNWs even over large turning tracks. In situ scanning electron microscopy stretching and electric transport characterizations reveal a robust and highly stretchable c-SiNW electric connection under huge stretching, more than 200% of its original channel length. This reliable batch-manufacturing and line-shape engineering strategy could provide a solid basis for large scale implementation of c-Si technology for future c-Si based wearable or biocomfortable electronic applications.

The SiNWs were grown upon oxide-coated Si wafers or glass substrates, via an in-plane solid−liquid−solid (IPSLS) growth mechanism,[31−36] where a hydrogenated amorphous Si thin film is deposited upon a substrate surface to serve as the precursor layer for the indium (In) catalyst droplets to absorb and produce c-Si NWs. First of all, as depicted schematically in Figure 1c, an array of guiding terrace steps, predesigned into horseshoe edge shape, were patterned by lithography and etching into the underlying oxide substrates to form a step of 60−150 nm deep. Then, at the end of the guiding edges, crossing In strips were evaporated and patterned, followed by a H_2 plasma treatment in a plasma enhanced chemical vapor deposition (PECVD) system at 300 °C to remove the surface oxide and form discrete In droplets resting close to the guiding step edges (Figure 1d). After that, a hydrogenated amorphous Si (a-Si:H) thin film was deposited by plasma enhanced chemical vapor deposition of pure SiH_4 gas to a thickness of 30 to 60 nm. Upon annealing at 350 °C in vacuum, the In droplets became molten again, and started to absorb nearby a-Si:H layer and precipitate crystalline SiNWs during their in-plane movement. The in-plane growth is driven in principle by a higher Gibbs energy in the a-Si:H layer compared to that in the as-produced c-Si NWs with δG = 0.1−0.15 eV.[37,38] It is interesting to note that the extra sidewall-coated a-Si:H upon the terrace step edge introduces an effective attraction to the in-plane movement of the In droplets and thus provides a convenient means to direct the in-plane growth routine of SiNWs to follow the predefined guiding edge lines.[39,40] More experimental details are available in Methods and in our previous works.[35,39,40]

Figure 2a−g shows the typical scanning electron microscopy (SEM) characterizations of the line-shape engineered in-plane SiNWs, which were grown along an array of predesigned horseshoe guiding patterns, with a period of 22 μm and the outer and inner track turning radii of 10 and 6 μm, respectively. It is remarkable that the in-plane guided growth of SiNWs, led by the In droplets, can be rather stable and faithful, following exactly the predesigned growth routines that comprise of a series of turning tracks, over a very long distance that even extends beyond >1000 μm, as witnessed in the SEM image presented in Figure 2b. This is indeed a prerequisite for the in-plane SiNWs to implement a set of programmable line-shape degree of freedom maneuvering. Close examination of the guided growth of in-plane SiNWs within the green-dashed rectangle zone are provided in Figure 2e−g. Interestingly enough, along each guiding step edge there is always one and only one SiNW following the turning track of the guiding edges. Note that the SiNWs, tinted with a pseudocolor of pale yellow in Figure 2f for vision clarity, feature a width of only 70−100 nm, lying close to but still well separated by a narrow gap of 10−20 nm from the terrace step edge (colored in green in Figure 2g). The formation of such a gap between the guided SiNW and the step edge is due to the fact that the leading In catalyst droplets are usually larger than the produced SiNWs. When the In droplet does touch the step edge during a guided in-plane growth, the produced SiNWs, which usually precipitate in the center of the rear SiNW/In interface, are thus separated from the step edge. This situation is particularly common to the relatively thick SiNWs produced by large In droplets as shown in this work.

The kicking-off growth of the in-plane SiNWs, found at the crossing between the In strips and the guiding edges, is also examined by SEM and shown in Figure 2c. While a high population of discrete In catalyst droplets (here typically 350 to 450 nm in diameter) are formed upon the 5 μm-wide In strip, only those located at the strip edge can pull out into the free space (that is, into the area with a-Si:H layer coating but no other competing droplets) and thus produce in-plane SiNWs. It is also noteworthy that, because there are always several In droplets formed along the guiding edge (in the crossing places as seen in Figure 2c), the chance for the step edge line to trap at least one of the nearby In droplets and to initiate a guided growth is found to be rather high (even close to unity). Then, once the In droplets ran into the guiding tracks and grew along the step edge, no other SiNWs can be guided along the same guiding edge. Indeed, the in-plane growth is self-avoiding due to the depletion of nearby a-Si:H layer along the growth path. This thus ensures that a single step edge will direct only one SiNW, as seen for instance in Figure 2c, where the growth route of the in-plane SiNW is indicated by the yellow-dashed line. In the meantime, other free or random in-plane SiNWs without the step-edge guidance are also observed around the In strips, but most of them ended up with self-trapping or stopped by running into nearby other SiNWs. Therefore, a directed growth along predefined guiding tracks is crucial to initiate a stable and continuous in-plane growth of ultralong SiNWs for further line-shape engineering. For example, according to a statistics of the length of 342 guided SiNWs found along the guiding tracks, see Supporting Information Figure S.1, more than 75% (or 12%) of the guided SiNWs can grow into a length of >500 μm (or >950 μm).

Empowered by this precise guided growth capability, the line-shape degree of freedom (DOF) of in-plane SiNWs can be explored to produce any singly connected 2D patterns that can be completed in a one-touch-drawing growth of the in-plane SiNWs. An example of this has been demonstrated in Figure 2d, where the in-plane SiNWs, starting from several separate In pads (as seen in the top-right SEM inset), are directed by the guiding step edges to grow directly into a Peano curve in its first order, with a half-vertical and half-horizontal layout design,[41] which is one of the best known fractal layouts that render large stretchability.[42] In addition, this line-shape engineering strategy is also applicable to produce a rich set of other nanowire patterns, as shown in the SEM images in the Supporting Information Figure S.3, where Figure S.3b shows that the in-plane growth of SiNWs can be controlled to steer even a sharp turning with local radius of only 500 nm. The continuous and faithful guided growth of a single SiNW around the full perimeter of a drop-shape island, as witnessed in Supporting Information Figure S.3d, highlights again the general capability of this in-plane engineering strategy to synthesize any noncrossing 2D pattern in a single run self-assembly growth.

DOI: 10.1021/acs.nanolett.7b03658
Nano Lett. 2017, 17, 7638−7646

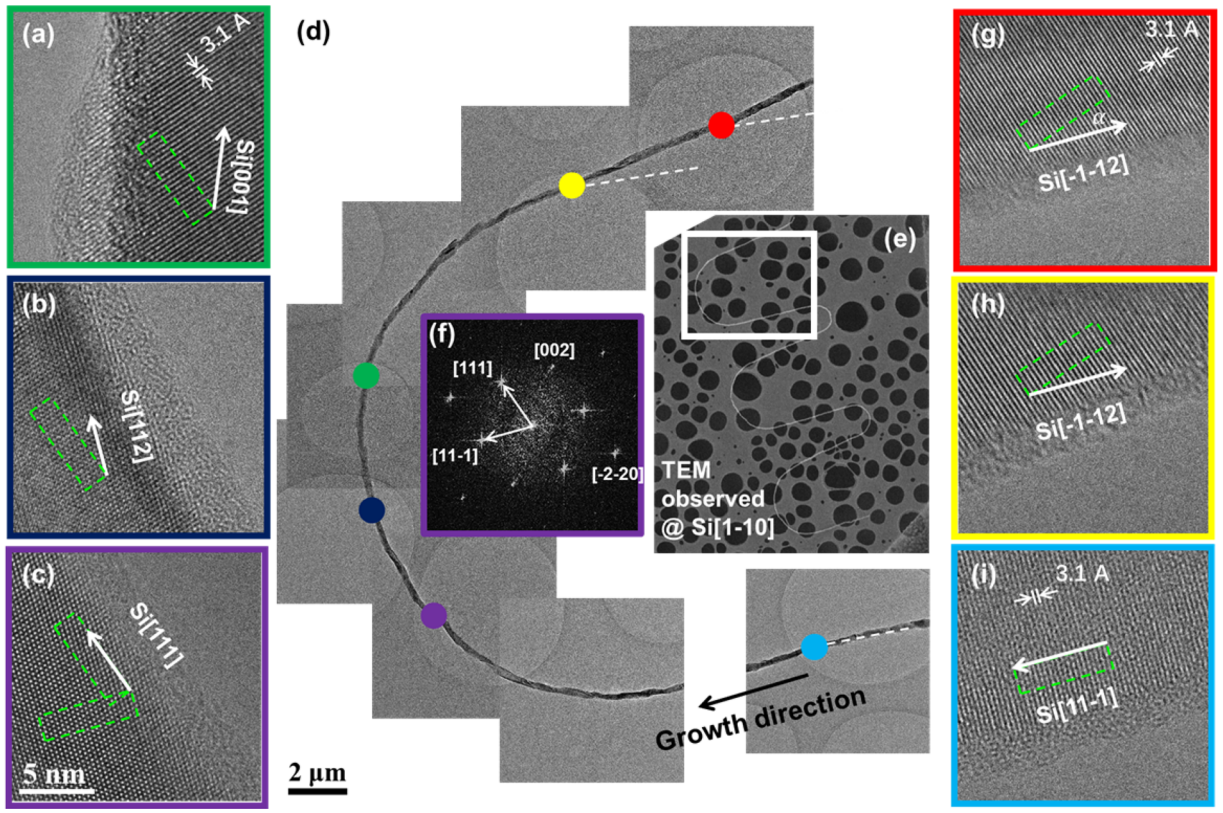

Figure 3. Structural analysis of an in-plane SiNW spring segment. (a–c,g–i) High-resolution transmission electron microscopy (HR-TEM) lattice images, taken at different places marked by the spots of corresponding colors along a SiNW bend, as seen in the overall TEM image in (d), which is a chosen zone from the ultralong SiNW spring in (e), with a fast Fourier transform converted selected area electron diffraction pattern displayed in (f).

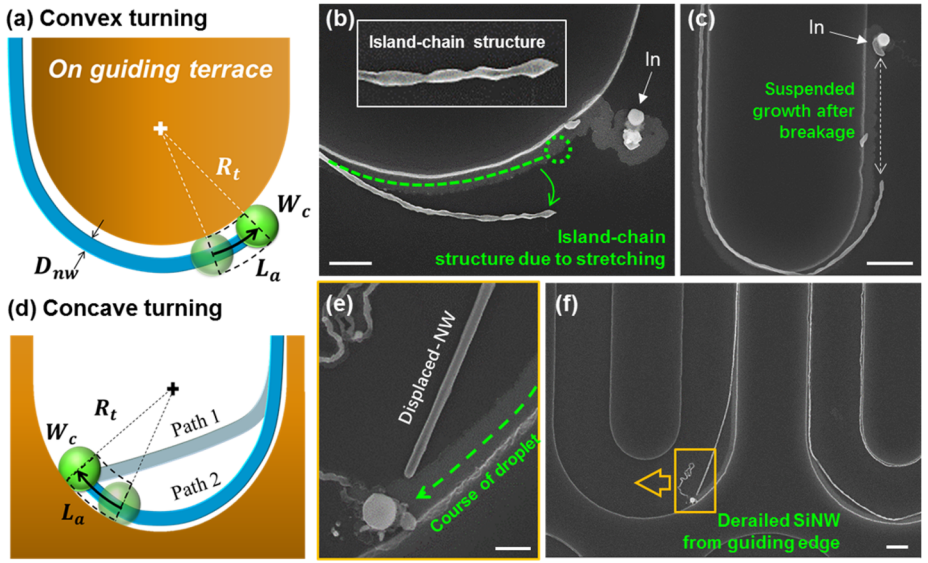

Figure 4. Growth stability at the convex or concave turnings. (a–d) The different edge-catalyst contact situations for a guided growth of SiNW, led by a catalyst droplet, at convex and concave turning tracks, respectively. (b,c) SEM images of the discontinuous guided growth of SiNWs due to decreased a-Si:H supply at a convex-turning track, and the island-chain structure resulted from a strong interface–pulling before breakage. (e,f) Situations for an unstable concave-turning growth that features instead a derailing of guided SiNWs due to pulling strain. The scale bars in (b,c,e,f) are 1 μm, 2 μm, 500 nm, and 2 μm, respectively.

The crystallinity and the structural quality of the line-shape engineered in-plane SiNWs were further investigated by using high-resolution transmission electron microscopy (HR-TEM) and presented in Figure 3. Thanks to the fact that there is no chemical bonding between the in-plane SiNWs and the nearby substrate or the guiding edges sidewall, a segment of the line-shape engineered SiNW spring, consisting of three cycles of bends as seen in Figure 3e, could be picked up by nanomanipulators and transferred to a copper grid for structural analysis. Surprisingly, despite of a large turning of

DOI: 10.1021/acs.nanolett.7b03658
Nano Lett. 2017, 17, 7638–7646

the SiNWs enforced by the guiding edge line, HR-TEM images taken at different places along the bent segment, displayed in Figure 3a–c and g–i (marked by different colors) reveal an almost coherent lattice arrangement throughout the whole turning of the SiNW. For example, along the growth direction indicated by the black arrow in Figure 3d, the local growth orientation of the SiNW, marked by the white arrows in the local lattice images at each place, is found to vary gradually from Si[11$\bar{1}$], to Si[111], to Si[112] and to Si[001] around the turning track, where the green-dashed rectangles are placed to highlight the alignment of the local Si ⟨111⟩ orientations. Only at the end of the upper branch, in the places marked by the red and the yellow spots, the local growth orientation seems to deviate slightly into Si[$\bar{1}$1$\bar{2}$]. Nevertheless, these findings indicate that the whole SiNW spring, grown over the U-turn track, is almost equivalent to a fine c-Si nanopiece carved out of a single crystal, whereas this has been simply accomplished in a single nanopulling growth led by an In droplet without the need of any external manipulation.

Though a guided growth of in-plane SiNWs along straight edges has been observed in our previous works,[40,43] implementing such precise growth routine control over programmed turning tracks with periodic large negative and positive curvatures has never been explored for the in-plane growth control of ultralong SiNWs. Actually, the impact of a curved guiding track is nontrivial and, as schematically depicted in Figure 4a,d, can lead to a modified absorption–deposition balance condition, and consequently different interface–stress and SiNW geometry as witnessed in the SEM images shown in Figure 4b,c,e,f. Considering the Si mass conservation in an In droplet advancing along a straight guiding edge, the absorption of Si atoms from the front interface should be equal to the deposition of Si atoms at the rear SiNW end, which can be formulated as

$$S_{\mathrm{abs}}^{\mathrm{straight}} = W_{\mathrm{c}}\cdot h_{\mathrm{a}} + h_{\mathrm{s}}\cdot h_{\mathrm{a}} \sim S_{dep} = D_{\mathrm{nw}}^2 = f^2\cdot W_{\mathrm{c}}^2 \tag{1}$$

where W_c is the width of In droplet, h_a is the a-Si:H layer thickness coated on the ground and the vertical sidewall, h_s is the height of the guiding edge, and $f = D_{nw}/W_c$ is the ratio between the diameter of SiNW and the cross section size of the In catalyst droplet, which is more or less a constant determined by the local surface tension force balance at the triple phase line.[33] Note that the formulation of S_{dep} applies to both cases of guided growth along straight or curved tracks.

In order to maintain a mass conservation, as stated in eq 1, the catalyst droplets should have a cross section diameter of $W_{c0} = \frac{h_a}{2f^2}(1 + \sqrt{1 + 4f^2 h_s/h_a})$. If the initial catalyst droplet is too large with diameter of $D_c > W_{c0}$, the liquid droplet will be forced to deform into an ellipse shape that can be approximated by an elongated cuboid of W_c wide and L_c long (measured along the growth direction) with $L_c > W_c$ and a constant catalyst volume of $V_c = W_c^2 L_c = D_c^3$. In this case, the front absorption and the rear deposition interfaces can be considered as exerting a stretching force to the liquid droplet sandwiched in between. In view of minimizing the exposed surface/interface energy, a roughly spherical shape of the In droplet is energetically preferable with $D_c = L_c$. As a consequence, given a constant a-Si:H layer thickness of h_a, the In droplets with more or less $D_c \sim W_{c0}$ will be effectively selected by this rule to initiate a stable guided growth along the tracks. This is indeed the case, as shown in Supporting Information Figure S.2, where statistics of the stable guided growth of the in-plane SiNWs against their diameters ($D_{nw} \sim W_c$) are presented, of different a-Si:H layer thicknesses of h_a = 25, 30, and 40 nm. It is clear that a thicker a-Si:H layer does preferentially activate the larger In droplets for guided growth, thus producing thicker SiNWs, but also demonstrate a broader dispersion in the size distribution. This finding is quite similar to the selective activation corridor found for the planar in-plane growth in our previous work.[44]

When the In droplet runs into a convex turning track, as depicted in Figure 4a, the advancement of the In droplet over an arc length of dL_a, or a turning angle of $d\theta \sim dL_a/(R_t + W_c/2)$ where R_t is the turning radius, will consume a volume amount of a-Si:H of

$$V_{\mathrm{a}} = \frac{d\theta}{2}((R_{\mathrm{t}} + W_{\mathrm{c}})^2 - R_{\mathrm{t}}^2)h_{\mathrm{a}} + d\theta R_{\mathrm{t}} h_{\mathrm{s}} h_{\mathrm{a}} \tag{2}$$

And thus, the absorption flux rate can be written as

$$S_{\mathrm{abs}}^{\mathrm{convex}} = \frac{dV_{\mathrm{a}}}{dL_{\mathrm{a}}} = W_{\mathrm{c}}h_{\mathrm{a}} + \left(1 - \frac{W_{\mathrm{c}}}{2R_{\mathrm{t}} + W_{\mathrm{c}}}\right)h_{\mathrm{s}}h_{\mathrm{a}} = S_{\mathrm{abs}}^{\mathrm{planar}} - \Delta S^{\mathrm{cv}} \tag{3}$$

where the first term on the right-hand side eq 3 is the same as that expressed in eq 1 for guided growth along straight track, while the second term stands for the decrease of the a-Si:H absorption on the curved convex guiding edge sidewall, by an amount of $\Delta S^{cv} = \frac{h_s h_a}{1 + 2R_t/W_c}$. Specifically, given a catalyst diameter of ∼400 nm, turning over a track with a radius of 4 μm will lead to a Si supply shortage close to 5% in the In droplet. In principle, this Si atom supply shortage experienced at a convex bending will lead to a slowdown of the rear deposition interface, with respect to the front absorption interface, and thus resulting in an interface–stretching or pulling force between the In droplet and the as-produced SiNW segment. As a consequence, as seen, for example, in Figure 4b,c, the leading In droplets could be detached from the SiNW end during its turning over a convex bend. The appearance of a series of island-chain SiNW structures, immediately before the breakage of the SiNW from the In droplet, as seen in Figure 4b and its inset, also hints at the existence of a significant interface-pulling force that is known to cause a catalyst-droplet-mediated Plateau-Rayleigh transformation of the SiNWs.[35] It is also critical to note that the perturbation of a-Si:H supply of $\Delta S^{cv} \sim \frac{1}{1 + 2R_t/W_c}$ experienced during turning over bend, is actually determined by the ratio between the turning radius over the diameter of catalyst R_t/W_c, instead of their absolute values. This means that a thinner SiNWs will find it easier to turn over a sharper bend, as witnessed indeed in the SEM images shown in Supporting Information Figure S.3b,d.

In contrast, when the In droplets grow over a concave turning track, as illustrated in Figure 4d, a net gain in Si atom supply is obtained, by $\Delta S^{cc} = h_s h_a/2(1 + R_t/W_c)$, thanks to a longer absorption contact length between the In droplet and the a-Si:H-coated step sidewall, as sketched in Figure 4d. Therefore, there is no such Si-supply shortage issue when an In droplet is directed into concave turning tracks. However, a new derailing situation could also happen, under tensile interface strain, as witnessed in Figure 4e,f, where the step-constrain in the inward direction (due to the convex turning track) is now lost. Remarkably, while the catalyst droplets are still observed to follow the predesigned guiding arc or track, as inferred from the lighter trench region along the guiding tracks, which result from

DOI: 10.1021/acs.nanolett.7b03658
Nano Lett. 2017, 17, 7638–7646

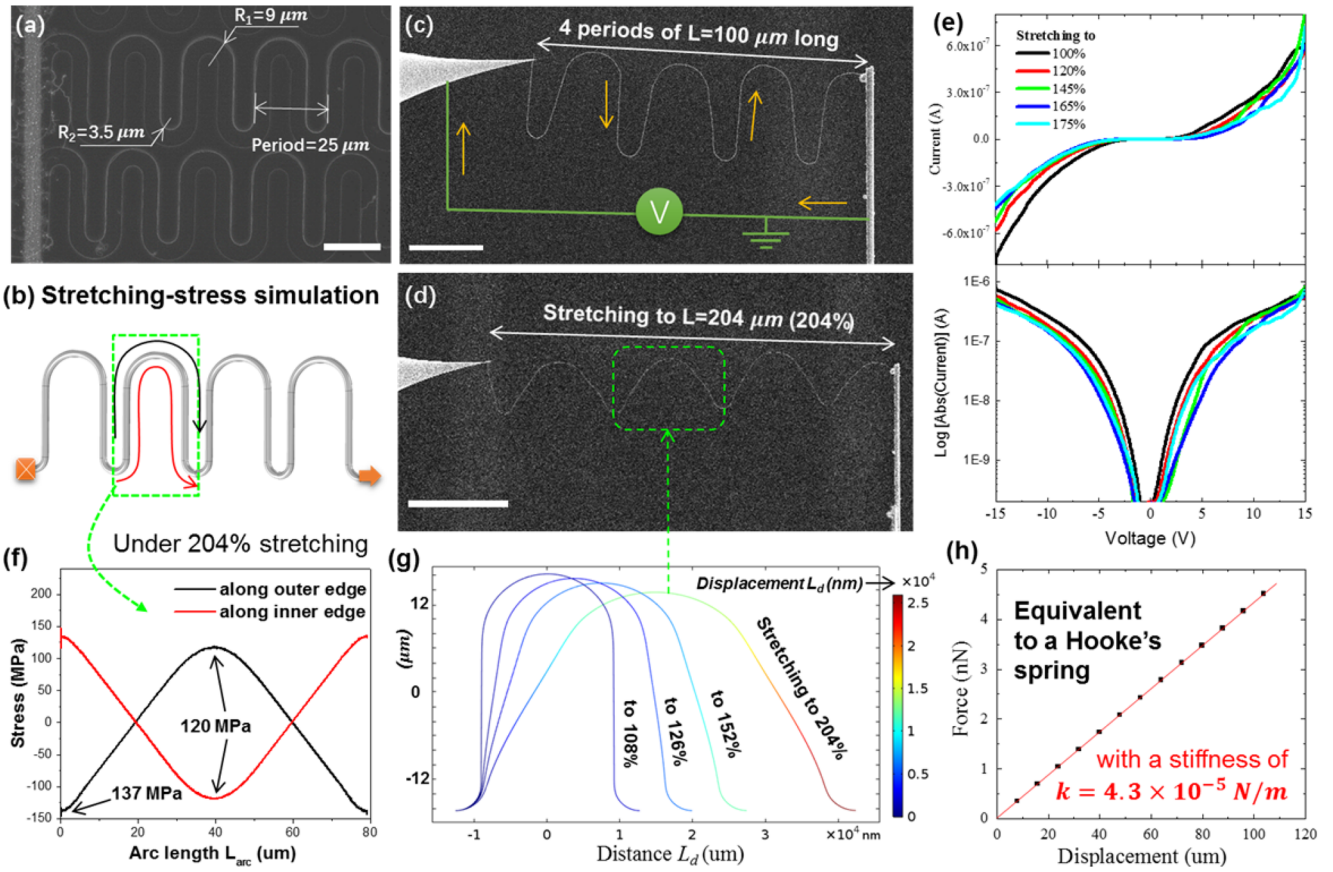

Figure 5. Stretching and electric transport testing of SiNW springs. (a) SEM image of the line-shaped engineered in-plane SiNWs with a period spanning 25 μm and two different bends of radii R_1 = 9 μm and R_2 = 3.5 μm, respectively. (c,d) SEM images of a SiNW spring segment mounted between two probes for in situ stretching and electric transport testing, while (e) shows the measured current−voltage curves under different stretching deformations. The scale bars in (a,c,d) are 20, 25, and 50 μm, respectively. (b) The chosen unit of a SiNW spring for finite element simulation and analysis, while (g) presents the geometry evolution of a SiNW spring unit subject to different stretching displacement. The stress distribution along the outer and the inner lines (marked as black and red in b) are extracted and plotted in (f). The simulated force−displacement relationship of the SiNW spring is presented in (h).

the absorption of a-Si:H layer and the exposure of the underlying substrate surface leading to a different contrast in SEM imaging, the produced in-plane SiNW can instead take a shortcut, by displacing from the guiding track and thus producing a sweeping, straight and thicker segment, as illustrated by the Path 1 in Figure 4d, compared to that of a faithful guided growth of Path 2. This peculiar phenomenon happens when the overall a-Si:H layer is slightly thinner than that required for a balance growth, and as a consequence a tensile strain develops during the in-plane guided growth and accumulates to become large enough to displace the SiNWs from their original tracks, but only taking place at the concave-turning bends.

These findings highlight the extraordinary impact of the interface−interaction forces on the guided growth stability and line-shape geometry of the in-plane SiNWs. Note that, this phenomenon only happens in a nanodroplet-mediated growth with a solid thin film precursor (IPSLS growth) but not in the typical VLS growth with a gas-feeding environment. This is because only a solid precursor (a-Si:H) forming an absorption interface in front can exert a significant interface-interaction force to distort the liquid catalyst droplet and impact the produced SiNWs. In order to achieve a faithful and programmable line-shape engineering, the tensile interface−pulling strain should be properly controlled by tuning the growth balance condition as stated in eq 1, particularly over sharp turnings. In general, a relatively thicker a-Si:H layer with respect to the diameter of leading catalyst droplet can help to offset the decrease of Si supply at the convex turnings and also avoid/suppress the derailing of SiNWs over the concave bends, as both of them result from an interface-pulling force during the in-plane guided growth.

As an example of the potential of this line-shape engineering capability, a segment of in-plane SiNW spring of ~100 nm in diameter, consisting of 4 periods of turnings with a total length of 100 μm (one period for a span of 25 μm with two bends of R_1 = 9μm and R_2 = 3.5 μm, as shown by the SEM image in Figure 5a), was first picked up from the guiding track by using a tungsten nanoprobe in the SEM chamber and then bonded to a conductive c-Si tip cantilever at the other end, as shown in Figure 5c.[45,46] Note that, as the bonding connections between the SiNW spring and the nanoprobe and the cantilever were realized by amorphous carbon (a-C) deposition in the environmental SEM system, therefore an Ohmic contact is not expected. Nevertheless, under different electric bias between the probe electrodes, the current through the SiNW spring can be recorded under different stretching strains. For example, the SEM image in Figure 5d shows the deformation of the SiNW spring into sinusoidal shape when being stretched to 204 μm long (or 204%) by the two electrodes, while the upper

DOI: 10.1021/acs.nanolett.7b03658
Nano Lett. 2017, 17, 7638−7646

and the lower panels in Figure 5e show, respectively, the linear and the logarithmic plots of the current−voltage (I−V) characteristics under different values of the stretching strains, ranging from 100% to 175%. It is important to note that the I−V curves only decrease slightly under larger and larger stretching strains, which could be assigned to the unstable electric contacts at the two ends bonded by a-C coating. Despite this, a robust electrical connection is provided to the highly stretchable SiNW springs. In addition, we note that, at the end of the stretching−IV testing, it is the connection between the spring and the cantilever, not the SiNW spring itself, that broke (as seen in Supporting Information Figure S.4). In another stretch test shown in Supporting Information Figure S.5, a SiNW spring has been stretched to an even larger extent of >270% that almost pulled the SiNW spring into a straight line. Remarkably enough, all these SiNW springs can quickly recover their original shape when the force is released.

A finite element modeling and simulation was also carried out, by using COMSOL suite, to investigate the stress/pressure distribution along the line-shape engineered SiNW springs. The simulation unit under consideration is indicated by the green dash rectangle in Figure 5b, where a pair of periodic boundary conditions were applied at the two ends, among them one is fixed while the other is subject to different lateral stretching. The SiNW is assumed to take on the typical anisotropic mechanical properties of bulk c-Si with a Young's Modulus of 170 GPa and Poisson's ratio of 0.28. Figure 5g shows the simulated gradual line-shape evolution of a single SiNW spring unit under gradually increased stretching displacement, up to 204%. Indeed, the last deformation does reproduce very well the experimental line-shape under 204% stretching observed in the SEM image shown in Figure 5d. In addition, the stress distributions along the outer and the inner edges, as marked by the red and black lines in Figure 5b respectively, are extracted and plotted in Figure 5f, where the maximum tensile or compressive stresses of ∼136 MPa are found at the small bends, while lower values ∼120 MPa are recorded on the larger turning. All these values are at least 1 order of magnitude lower than the fracture strength in crystalline Si, which is typically 2 to 10 GPa.[47,48] As a consequence, the line-shape engineered SiNW can behave like an extremely soft but resilient spring, which is predicted by simulation to deliver a linear mechanic response following typical Hooke's law and with a very low stiffness of $k = 4.3 \times 10^{-5}$ N/m, as shown in Figure 5h.

In analogy to the crystal pulling of Si ingot from molten liquid (at >1400 °C), as depicted schematically in Figure 1a, the in-plane growth of SiNWs can be considered as a nanoscale crystal pulling from the molten nanodroplets that are loaded with supersaturated Si atoms, as illustrated in Figure 1b. During this course, a continuous growth and natural extension of the c-Si segment from the solid (c-Si) /liquid (droplet) deposition interface is crucial for achieving a coherent lattice ordering in the as-produced SiNWs. As the moving catalyst droplets are tiny and flexible for manipulation, a high quality line-shape engineering becomes now possible at a much lower growth temperature <350 °C, only with the aid of programmable terrace edge lines that can be easily defined without the need of sophisticated high resolution lithography. This provides a reliable, low-cost and deterministic strategy to extend the well-established c-Si technology into the rapidly emerging flexible and stretchable electronics, where the ultralong SiNWs could serve not only as elastic electric connections, and but also as active semiconducting channels which are indispensable for logic and sensor applications.

Meanwhile, it is very important to note that, the stretchability achieved by a serpentine or zigzag meander channel design is further limited by a scale factor of $s = R_t/W_c$, where R_t and W_c are the turning radius and the width of the channel (for SiNW, $W_c = D_{nw}$), respectively. A higher scale factor, typically $s > 10$ for a stretchability of 20%,[49,50] is preferable to avoid stress accumulation (that will lead to crack formation or fracture) or out-of-plane buckling. In top-down lithography or patterning approaches, the channel width is limited by the lithography resolution. Thus, the small diameter of the in-plane SiNWs, readily controllable in the range of 30−100 nm by tuning the initial catalyst formation,[31,35,43] represents an important advantage to achieve a high scale factor, for instance $s = 10^2$ to 10^3 for the SiNW springs shown in Figure 2 and Figure 5, to enable highly stretchable and elastic electronics.

Finally, it is also important to note that the implementation of the line-shape engineered SiNWs for stretchable electronics will require a transferring of the springs from the growth substrate to a soft carrier. To this end, a precise growth location, routine, and pattern control of the planar SiNW array provide an important basis to achieve a reliable batch-transferring. In Supporting Information Figure S.6a, we show that the pictures of SiNW springs connected, by round Pt/Au electrodes, which are safely transferred to soft polydimethylsiloxane (PDMS) elastomer. This has been done simply by casting a PDMS layer of 10 μm thick over the SiNW spring/SiO_2 (300 nm)/c-Si wafer sample, followed by a 4% HF solution dipping to etch off the oxide layer and release the PDMS layer that carries the SiNW springs and the Pt/Au electrodes all together. Such an easy picking and transferring of the in-plane SiNWs has been enabled by the fact that the as-grown SiNWs are not bonded to the substrate and thus easy to harvest by standard polymer transferring procedure. In Supporting Information Figure S.6a, the SiNW springs are identified as the bright spring lines, bridging the round metal electrodes. Note that the apparent width of the SiNWs under optical microscope (due to the scattering of light by the high refractive-index SiNW) is much thicker than their actual physical size. Interestingly, the transferred SiNW springs are also found to be highly resilient when subject to the distortion of displaced Pt/Au electrodes, as witnessed in the photograph shown in Supporting Information Figure S.6b. While further improvement of the batch-transferring technique is required, these observations support that the line-shape engineered SiNW springs could serve as a promising semiconducting material for future stretchable electronics.

In summary, we have demonstrated a deterministic and programmable line-shape engineering of ultralong SiNWs, produced by a reliable indium droplet mediated in-plane solid−liquid−solid growth mechanism. This unique capability has been explored to batch-manufacture an orderly array of highly stretchable SiNW springs and arbitrary singly connected 2D patterns. HR-TEM analysis reveals a monolike high crystalline quality in the SiNW spring over continuous turning tracks, thanks to a gentle nanocrystal-pulling growth from the running catalyst droplet. Strikingly, the SiNW springs are found to be extremely stretchable >270% and elastic, while carrying a robust electric current, as testified by in situ SEM probe manipulation and I−V testing. This programmable line-shape engineering capability could eventually enable a new generation

DOI: 10.1021/acs.nanolett.7b03658
Nano Lett. 2017, 17, 7638−7646

of stretchable sensing and even logic electronics that inherits the high performance from c-Si based electronics.

Methods. *Substrate Preparing and Guiding Edge Patterning.* The in-plane SiNWs are grown on glass substrates or Si(100) wafers covered with 300 nm silicon oxide layer, which were cleaned with standard RCA procedures prior to experiments. The predesigned guiding terrace edges were patterned via lithography and subsequent reactive ion etching (RIE) into the underlying SiO_2 layer to a depth of 150 nm. The In strip lines, crossing the guiding edge lines, were defined by lithography and then thermal evaporation to a thickness of 30 to 50 nm.

Indium Droplet Formation and SiNW Growth. The sample was loaded into the chamber of a PECVD system, where a H_2 plasma treatment is applied at 300 °C, with 100 SCCM flow rate, 100 Pa chamber pressure and 125 mW/cm^2 RF power density. During this process, the surface oxide layer on the In strips was reduced and the In thin film was allowed to agglomerate into discrete droplets of 200 to 400 nm. Hydrogenated amorphous Si (a-Si:H) was deposited at 100 to 150 °C by the decomposition of 10 SCCM of pure SiH_4 in the plasma with 60 Pa pressure and 60 mW/cm^2 to a layer thickness of 20−32 nm. Upon a simple vacuum annealing at 350 to 450 °C for 1 h, the In droplets became molten again and started to move laterally. During this course, the In droplets that ran into the guiding edge lines will be attracted by the extra amorphous layer on the vertical step sidewall and thus moved along the step edge into predesigned line-shapes.

In Situ Mechanical Testing and I−V Measurement. The SiNW spring was handled by using a nanomanipulator (Kleindiek MM3A) in a SEM system, being mounted at one end to a Si cantilever (Veeco CLFC-NOBO) and the other to a tungsten probe tip, as seen in the SEM image shown in Figure 5c. During the stretching, a bias was applied between the probe and the cantilever while the current was recorded by the connected source-monitor unit (B1500A Semiconductor Device Parameter Analyzer).

■ ASSOCIATED CONTENT

Supporting Information

The Supporting Information is available free of charge on the ACS Publications website at DOI: 10.1021/acs.nanolett.7b03658.

Statistics over the length and the diameter distributions of the guided in-plane SiNWs; SEM images of the line-shape engineering controls of the in-plane SiNWs along different 2D growth track pattern designs; SEM snapshots of SiNW springs stretched by two nanoprobes; Photographs of the SiNW springs, connected by Pt/Au electrode pads, transferred to soft substrate (PDF)

■ AUTHOR INFORMATION

Corresponding Authors

*E-mail: weixl@pku.edu.cn (X.W.)
*E-mail: yulinwei@nju.edu.cn (L.Y.)

ORCID

Zhaoguo Xue: 0000-0002-5514-885X
Linwei Yu: 0000-0002-0801-5210
Qing Chen: 0000-0002-7919-5159
Pere Roca i Cabarrocas: 0000-0003-2241-2762

Notes

The authors declare no competing financial interest.

■ ACKNOWLEDGMENTS

The authors acknowledge the financial support from the National Basic Research 973 Program under Grant 2014CB921101, the NSFC under 61674075, the National Key Research and Development Program of China grant 2017YFA0205003, the Jiangsu Excellent Young Scholar Program under BK20160020, the Scientific and Technological Support Program in Jiangsu province under BE2014147-2, Jiangsu Shuangchuang Team's Personal Program and the Fundamental Research Funds for the Central Universities. Z.X. acknowledges the financial support from China Scholarship Council and the Postgraduate Program of Jiangsu Province KYZZ160052.

■ REFERENCES

(1) Kim, J.; Salvatore, G. A.; Araki, H.; Chiarelli, A. M.; Xie, Z.; Banks, A.; Sheng, X.; Liu, Y.; Lee, J. W.; Jang, K.-I.; et al. *Science advances* **2016**, *2* (8), e1600418.
(2) Xu, B.; Rogers, J. A. *Extreme Mechanics Letters* **2016**, *7*, 44−48.
(3) Kim, D.-H.; Ghaffari, R.; Lu, N.; Rogers, J. A. *Annu. Rev. Biomed. Eng.* **2012**, *14*, 113−128.
(4) Hussain, A. M.; Hussain, M. M. *Adv. Mater.* **2016**, *28* (22), 4219−4249.
(5) Hammock, M. L.; Chortos, A.; Tee, B. C. K.; Tok, J. B. H.; Bao, Z. *Adv. Mater.* **2013**, *25* (42), 5997−6038.
(6) Cheng, T.; Zhang, Y.; Lai, W. Y.; Huang, W. *Adv. Mater.* **2015**, *27* (22), 3349−3376.
(7) Wang, Y.; Zhu, C.; Pfattner, R.; Yan, H.; Jin, L.; Chen, S.; Molina-Lopez, F.; Lissel, F.; Liu, J.; Rabiah, N. I.; Chen, Z.; Chung, J. W.; Linder, C.; Toney, M. F.; Murmann, B.; Bao, Z. *Science Advances* **2017**, *3* (3), e1602076.
(8) Roberts, M. E.; Mannsfeld, S. C. B.; Stoltenberg, R. M.; Bao, Z. *Org. Electron.* **2009**, *10* (3), 377−383.
(9) Sokolov, A. N.; Roberts, M. E.; Bao, Z. *Mater. Today* **2009**, *12* (9), 12−20.
(10) Arias, A. C.; MacKenzie, J. D.; McCulloch, I.; Rivnay, J.; Salleo, A. *Chem. Rev.* **2010**, *110* (1), 3−24.
(11) Lei, Z.; Wang, Q.; Sun, S.; Zhu, W.; Wu, P. *Adv. Mater.* **2017**.
(12) Lin, P.; Yan, F. *Adv. Mater.* **2012**, *24* (1), 34−51.
(13) Sepulveda, A. C. C.; Cordero, M. S. D.; Carreño, A. A. A.; Nassar, J. M.; Hussain, M. M. *Appl. Phys. Lett.* **2017**, *110* (13), 134103.
(14) Rojas, J. P.; Arevalo, A.; Foulds, I. G.; Hussain, M. M. *Appl. Phys. Lett.* **2014**, *105* (15), 154101.
(15) Kim, J.; Lee, M.; Shim, H. J.; Ghaffari, R.; Cho, H. R.; Son, D.; Jung, Y. H.; Soh, M.; Choi, C.; Jung, S. *Nat. Commun.* **2014**, *5*, 5747.
(16) Khang, D.-Y.; Jiang, H.; Huang, Y.; Rogers, J. A. *Science* **2006**, *311* (5758), 208−212.
(17) Kim, D.-H.; Ahn, J.-H.; Choi, W. M.; Kim, H.-S.; Kim, T.-H.; Song, J.; Huang, Y. Y.; Liu, Z.; Lu, C.; Rogers, J. A. *Science* **2008**, *320* (5875), 507−511.
(18) Jang, K.-I.; Li, K.; Chung, H. U.; Xu, S.; Jung, H. N.; Yang, Y.; Kwak, J. W.; Jung, H. H.; Song, J.; Yang, C.; et al. *Nat. Commun.* **2017**, *8*, x.
(19) Wagner, R. S.; Ellis, W. C. *Appl. Phys. Lett.* **1964**, *4* (5), 89.
(20) Dhalluin, F.; Baron, T.; Ferret, P.; Salem, B.; Gentile, P.; Harmand, J. C. *Appl. Phys. Lett.* **2010**, *96* (13), 133109−3.
(21) Ryu, S. Y.; Xiao, J.; Park, W. I.; Son, K. S.; Huang, Y. Y.; Paik, U.; Rogers, J. A. *Nano Lett.* **2009**, *9* (9), 3214−3219.
(22) Xu, F.; Lu, W.; Zhu, Y. *ACS Nano* **2011**, *5* (1), 672−678.
(23) Durham, J. W.; Zhu, Y. *ACS Appl. Mater. Interfaces* **2013**, *5* (2), 256−261.
(24) Pevzner, A.; Engel, Y.; Elnathan, R.; Tsukernik, A.; Barkay, Z.; Patolsky, F. *Nano Lett.* **2012**, *12* (1), 7−12.

DOI: 10.1021/acs.nanolett.7b03658
Nano Lett. 2017, 17, 7638−7646

(25) Musin, I. R.; Boyuk, D. S.; Filler, M. A. *J. Vac. Sci. Technol., B: Nanotechnol. Microelectron.: Mater., Process., Meas., Phenom.* **2013**, *31* (2), 020603.
(26) Swain, B. S.; Lee, S. S.; Lee, S. H.; Swain, B. P.; Hwang, N. M. *J. Cryst. Growth* **2011**, *327* (1), 276−280.
(27) Tang, Y. H.; Zhang, Y. F.; Wang, N.; Lee, C. S.; Han, X. D.; Bello, I.; Lee, S. T. *J. Appl. Phys.* **1999**, *85* (11), 7981−7983.
(28) Tian, B.; Xie, P.; Kempa, T. J.; Bell, D. C.; Lieber, C. M. *Nat. Nanotechnol.* **2009**, *4* (12), 824−829.
(29) Lugstein, A.; Steinmair, M.; Hyun, Y. J.; Hauer, G.; Pongratz, P.; Bertagnolli, E. *Nano Lett.* **2008**, *8* (8), 2310−4.
(30) Musin, I. R.; Filler, M. A. *Nano Lett.* **2012**, *12* (7), 3363−3368.
(31) Xue, Z.; Xu, M.; Li, X.; Wang, J.; Jiang, X.; Wei, X.; Yu, L.; Chen, Q.; Wang, J.; Xu, J.; Chen, K.; Roca i Cabarrocas, P. *Adv. Funct. Mater.* **2016**, *26* (29), 5352−5359.
(32) Yu, L.; Alet, P.-J.; Picardi, G.; Roca i Cabarrocas, P. *Phys. Rev. Lett.* **2009**, *102* (12), 125501.
(33) Yu, L.; Roca i Cabarrocas, P. *Phys. Rev. B: Condens. Matter Mater. Phys.* **2010**, *81* (8), 085323.
(34) Chen, W.; Yu, L.; Misra, S.; Fan, Z.; Pareige, P.; Patriarche, G.; Bouchoule, S.; Cabarrocas, P. R. i. *Nat. Commun.* **2014**, *5*, 4134.
(35) Xue, Z.; Xu, M.; Zhao, Y.; Wang, J.; Jiang, X.; Yu, L.; Wang, J.; Xu, J.; Shi, Y.; Chen, K.; Roca i Cabarrocas, P. *Nat. Commun.* **2016**, *7*, 12836.
(36) Xu, M.; Xue, Z.; Wang, J.; Zhao, Y.; Duan, Y.; Zhu, G.; Yu, L.; Xu, J.; Wang, J.; Shi, Y.; Kunji, C.; Roca i Cabarrocas, P. *Nano Lett.* **2016**, *16* (12), 7317−7324.
(37) Štich, I.; Car, R.; Parrinello, M. *Phys. Rev. B: Condens. Matter Mater. Phys.* **1991**, *44* (20), 11092.
(38) Roorda, S.; Doorn, S.; Sinke, W. C.; Scholte, P. M. L. O.; van Loenen, E. *Phys. Rev. Lett.* **1989**, *62* (16), 1880.
(39) Yu, L.; Chen, W.; O'Donnell, B.; Patriarche, G.; Bouchoule, S.; Pareige, P.; Rogel, R.; Salaun, A. C.; Pichon, L.; Roca i Cabarrocas, P. *Appl. Phys. Lett.* **2011**, *99* (20), 203104−3.
(40) Xu, M.; Wang, J.; Xue, Z.; Wang, J.; Feng, P.; Yu, L.; Xu, J.; Shi, Y.; Chen, K.; Roca i Cabarrocas, P. *Nanoscale* **2017**, *9*, 10350.
(41) Fan, J. A.; Yeo, W.-H.; Su, Y.; Hattori, Y.; Lee, W.; Jung, S.-Y.; Zhang, Y.; Liu, Z.; Cheng, H.; Falgout, L. *Nat. Commun.* **2014**, *5*, 3266.
(42) Sagan, H. *Space-filling curves*; Springer Science & Business Media, 2012.
(43) Yu, L.; Oudwan, M.; Moustapha, O.; Franck, F.; Roca i Cabarrocas, P. *Appl. Phys. Lett.* **2009**, *95* (11), 113106.
(44) Yu, L.; Roca i Cabarrocas, P. *Phys. Rev. B: Condens. Matter Mater. Phys.* **2009**, *80* (8), 085313−5.
(45) Li, X.; Wei, X.; Xu, T.; Pan, D.; Zhao, J.; Chen, Q. *Adv. Mater.* **2015**, *27* (18), 2852−8.
(46) Li, X.; Wei, X. L.; Xu, T. T.; Ning, Z. Y.; Shu, J. P.; Wang, X. Y.; Pan, D.; Zhao, J. H.; Yang, T.; Chen, Q. *Appl. Phys. Lett.* **2014**, *104* (10), 103110.
(47) Zhu, Y.; Xu, F.; Qin, Q.; Fung, W. Y.; Lu, W. *Nano Lett.* **2009**, *9* (11), 3934−3939.
(48) O'Mara, W.; Herring, R. B.; Hunt, L. P. *Handbook of semiconductor silicon technology*; Crest Publishing House, 2007.
(49) Gonzalez, M.; Axisa, F.; Bulcke, M. V.; Brosteaux, D.; Vandevelde, B.; Vanfleteren, J. *Microelectron. Reliab.* **2008**, *48* (6), 825−832.
(50) Vanfleteren, J.; Gonzalez, M.; Bossuyt, F.; Hsu, Y.-Y.; Vervust, T.; De Wolf, I.; Jablonski, M. *MRS Bull.* **2012**, *37* (3), 254−260.

DOI: 10.1021/acs.nanolett.7b03658
Nano Lett. 2017, 17, 7638−7646